Sparse linear modeling of next-generation mRNA sequencing (RNA-Seq) data for isoform discovery and abundance estimation

Jingyi Jessica Li (李婧翌)[a], Ci-Ren Jiang[b], James B. Brown[a], Haiyan Huang[a,1], and Peter J. Bickel[a,1]

[a]Department of Statistics, University of California, Berkeley, CA 94720; and [b]Statistical and Applied Mathematical Sciences Institute, Research Triangle Park, NC 27709-4006

Contributed by Peter J. Bickel, September 25, 2011 (sent for review June 22, 2011)

Since the inception of next-generation mRNA sequencing (RNA-Seq) technology, various attempts have been made to utilize RNA-Seq data in assembling full-length mRNA isoforms de novo and estimating abundance of isoforms. However, for genes with more than a few exons, the problem tends to be challenging and often involves identifiability issues in statistical modeling. We have developed a statistical method called "sparse linear modeling of RNA-Seq data for isoform discovery and abundance estimation" (SLIDE) that takes exon boundaries and RNA-Seq data as input to discern the set of mRNA isoforms that are most likely to present in an RNA-Seq sample. SLIDE is based on a linear model with a design matrix that models the sampling probability of RNA-Seq reads from different mRNA isoforms. To tackle the model unidentifiability issue, SLIDE uses a modified Lasso procedure for parameter estimation. Compared with deterministic isoform assembly algorithms (e.g., Cufflinks), SLIDE considers the stochastic aspects of RNA-Seq reads in exons from different isoforms and thus has increased power in detecting more novel isoforms. Another advantage of SLIDE is its flexibility of incorporating other transcriptomic data such as RACE, CAGE, and EST into its model to further increase isoform discovery accuracy. SLIDE can also work downstream of other RNA-Seq assembly algorithms to integrate newly discovered genes and exons. Besides isoform discovery, SLIDE sequentially uses the same linear model to estimate the abundance of discovered isoforms. Simulation and real data studies show that SLIDE performs as well as or better than major competitors in both isoform discovery and abundance estimation. The SLIDE software package is available at https://sites.google.com/site/jingyijli/SLIDE.zip.

mRNA isoform discovery | single-end vs. paired-end sequencing | fragment length distribution | GC contents | penalized estimation

The recently developed next-generation mRNA sequencing (RNA-Seq) assay, with deep coverage and base level resolution, has provided a view of eukaryotic transcriptomes of unprecedented detail and clarity. Unlike microarrays, RNA-Seq data have novel splice junction information in addition to gene expression, thus facilitating whole-transcriptome assembly and mRNA isoform quantification. RNA-Seq data includes both single-end and paired-end reads, where a single-end read is a sequenced end of a cDNA fragment from an mRNA transcript, and a paired-end read is a mate pair corresponding to both ends of a cDNA fragment.

In the mRNA isoform discovery field, one of the most widely used software packages is Cufflinks (1). It builds a set of genes and exons solely from RNA-Seq data first, and subsequently uses a deterministic approach to find a minimal set of isoforms that can explain all the cDNA fragments indicated by paired-end reads. Cufflinks mainly uses qualitative exon expression and junction information in its isoform discovery, lacking a quantitative consideration of RNA-Seq data. Although Cufflinks gives very useful results, we note that the isoforms it discovers based on de novo assembled genes and exons can be heavily biased by different types of RNA-Seq data noise (2–5). Two recently published modENCODE (Model Organism Encyclopedia of DNA Elements) (6) consortium papers (7, 8) also raise concerns about relying solely on RNA-Seq reads in isoform discovery and have suggested using manual annotations to scrutinize the results.

In the mRNA isoform quantification field, the question is to estimate the abundance of isoforms in a given set. Available abundance estimation methods include direct computation (9, 10) and model-based approaches. Many model-based studies (1, 11–14) have used maximum-likelihood approaches to estimate isoform abundance. There are also efforts on formulating the abundance estimation problem as a linear model (15), where the independent and dependent variables are isoform expression levels and categorized RNA-Seq read counts, respectively. In particular, binary values have been used in the design matrix to relate categorized reads to different isoforms, but that design matrix misses the quantitative relationship between read quantities and isoform abundance.

In this study, we propose a statistical method called "sparse linear modeling of RNA-Seq data for isoform discovery and abundance estimation" (SLIDE) that uses RNA-Seq data to discover mRNA isoforms given an extant annotation of gene and exon boundaries, and to estimate the abundance of the discovered or other specified mRNA isoforms. The extant annotation can come from annotation databases [e.g., Ensembl (16) or UCSC Genome Browser (17)], can be supplemented by other transcriptomic data such as RACE or CAGE (18, 19), or can even be inferred from RNA-seq de novo assembly algorithms (1, 20). SLIDE is based on a linear model with a nonbinary design matrix modeling the sampling probability of RNA-Seq reads from mRNA isoforms. When modeling the design matrix, we considered the effects of GC content, cDNA fragment lengths, and read starting positions. This linear model, coupled with the carefully defined design matrix, gives SLIDE a stochastic property of making use of exon expression quantitatively in isoform discovery. The SLIDE model can also be easily extended to incorporate other transcriptomic data [e.g., RACE (18), CAGE (19), and EST (21)] with RNA-Seq to achieve more comprehensive results. The SLIDE software package is available at https://sites.google.com/site/jingyijli/SLIDE.zip.

Author contributions: J.J.L., C.-R.J., H.H., and P.J.B. designed research; J.J.L., C.-R.J., and H.H. performed research; J.J.L. and C.-R.J. contributed new reagents/analytic tools; J.J.L., C.-R.J., and H.H. analyzed data; and J.J.L., J.B.B., H.H., and P.J.B. wrote the paper.

The authors declare no conflict of interest.

Data deposition: The sequences reported in this paper have been deposited in the Sequence Read Archive, http://www.ncbi.nlm.nih.gov/sra (accession nos. SRX003838, SRX003839, SRX003836, SRX003837, SRR070261, SRR070269, SRR111873, SRR023600, SRR035402, SRR023720, SRR023715, SRR023751, SRR023707, and SRR023826).

[1]To whom correspondence may be addressed. E-mail: bickel@stat.berkeley.edu or hhuang@stat.berkeley.edu.

This article contains supporting information online at www.pnas.org/lookup/suppl/doi:10.1073/pnas.1113972108/-/DCSupplemental.

Results

Linear Modeling for RNA-Seq Data. SLIDE is designed as a tool for discovering mRNA isoforms and estimating isoform abundance from RNA-Seq reads, on top of known information about gene and exon boundaries. For isoform discovery, SLIDE considers all the possible isoforms by enumerating exons of every gene. For example, a gene of n nonoverlapping exons has $2^n - 1$ possible isoforms, each composed of a subset of the n exons. However, because of the possible occurrence of alternative splicing within exons, isoforms of the same gene may have partially overlapping but different exons. Hence, for ease of enumeration, we define a subexon as a transcribed region between adjacent splicing sites in any annotated mRNA isoforms (Fig. 1*A*). With this definition, every gene has a set of nonoverlapping subexons, from which we can enumerate all the possible isoforms including annotated ones.

We formulate the task of discovering isoforms for a given gene as a sparse estimation problem where the sparseness applies to the isoforms expected from RNA-Seq data. Because exon expression levels and the existence of possible exon–exon junctions are the key for isoform discovery and they can be inferred from the starting and ending positions of RNA-Seq reads mapped to a reference genome, we are motivated to transform RNA-Seq reads into a summary that captures the key information. For a paired-end read, we exact four genomic locations s_1, e_1, s_2, and e_2, where s_1 and e_1 are the starting and ending positions of its 5′ end, and s_2 and e_2 are the starting and ending positions of its 3′ end (Fig. 1*B*). Note that a paired-end read uniquely corresponds to a cDNA fragment with both ends sequenced, that is, s_1 and e_2 are the starting and ending positions of the fragment, respectively. We next categorize paired-end reads into paired-end bins defined as four-dimensional vectors: Bin (i, j, k, l) contains reads whose s_1, e_1, s_2, and e_2 are in subexons i, j, k ,and l, respectively (see *Methods* for details). For single-end reads, we can similarly categorize them into two-dimensional single-end bins. The so-defined bin counts provide all the exon expression and junction information.

SLIDE is built upon a linear model whose design matrix **F** models conditional probabilities of observing reads in different bins given an isoform. For paired-end data, modeling **F** requires distributional assumptions on the two ends (i.e., s_1, e_2) of a cDNA fragment in an mRNA transcript, or equivalently on the fragment's 5′ end (i.e., s_1) and its length (i.e., $e_2 - s_1$). For s_1, uniform distribution assumptions have been widely used. However, after considering the high correlation observed between sequencing read coverage and genome GC content (2), we assume the density of s_1 is uniform within subexons and proportional to the GC content between subexons. We specify the distribution of the fragment length, $e_2 - s_1$, by assuming e_2 to follow a Poisson point process given s_1 fixed. Consequently, $e_2 - s_1$ is modeled as truncated Exponential after taking into account the size selection step in RNA-Seq protocols (see *Methods*). Another widely used fragment length distribution is Normal distribution (1), which is also implemented in SLIDE and compared with truncated Exponential (see *SI Text*).

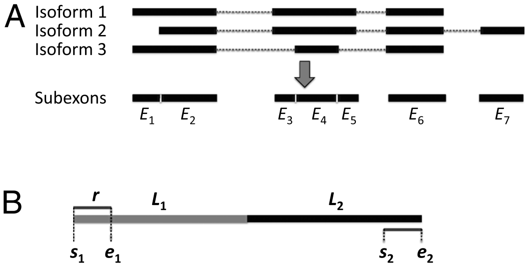

Fig. 1. (*A*) Definition of subexons: transcribed regions between adjacent alternative splicing sites. (*B*) A two-exon mRNA transcript. s_1, e_1, s_2, and e_2, genomic positions associated with a paired-end read. r, the read end length; L_1 and L_2, the exon lengths.

We then use a linear model as approximation to the observed bin proportions,

$$b_j = \sum_{k=1}^{K} F_{jk} p_k + \epsilon_j, \qquad j = 1, \cdots, J, \qquad [1]$$

where b_j is the observed proportion of reads in the jth bin, $F_{jk} = \Pr(j\text{th bin}|k\text{th isoform})$ (i.e., the conditional probability of observing paired-end reads in the jth bin given that they are from the kth isoform), p_k is the proportion of the kth isoform to be estimated, and ϵ_j is the error term with mean 0. Besides, J and K are the numbers of bins and isoforms, respectively (see *Methods*). This is the core linear model used in SLIDE for both isoform discovery and abundance estimation of discovered isoforms. For isoform discovery, usually $K > J$, so the model is unidentifiable. But based on biological knowledge, we expect the model to be sparse and achieve sparse estimation by a modified Lasso (22) method (see *Methods*). For abundance estimation, only the proportions of discovered isoforms are parameters in the linear model, and their number is often far less than K, so there is no identifiability issue anymore. SLIDE then does the parameter estimation by nonnegative least squares. Compared with maximum-likelihood approaches used by other abundance estimation methods, SLIDE has the computational advantage of fitting a linear model as an intrinsic element.

Simulation Results. A simulation study is used to assess the accuracy of SLIDE on isoform discovery and abundance estimation. We simulated reads from genes and true mRNA isoforms extracted from *Drosophila melanogaster* annotation (September 2010) of UCSC Genome Browser (17). For illustration purposes, we focus on the 3,421 genes on chr3R. Based on our defined subexons, those genes consist of 34.2% with 1–2 subexons, 57.6% with 3–10 subexons, and 8.2% with more than 10 subexons. Because the estimation for genes with 1–2 subexons is trivial due to their small numbers of possible isoforms, and genes with more than 10 subexons only constitute a small proportion and their estimation is computationally costly, we applied SLIDE to the subset of 3–10 subexons, 1,972 genes in total. We generated 500 × 50 (runs) paired-end reads for each gene from annotated isoforms of randomly defined proportions, and then we applied SLIDE to the simulated reads for isoform discovery and abundance estimation.

The isoform discovery results of all 50 runs are in Fig. 2*A*. We divided genes into groups by their numbers of subexons n ($n = 3, \cdots, 10$). For each gene, SLIDE returns a vector of estimated proportions of all its possible isofoms. We define isoforms whose estimated proportions exceed threshold 0.1 as discovered isoforms and evaluate them by the UCSC annotation. (Note that other thresholds 0.05 and 0.2 return similar results.) For each gene, the precision rate is defined as $TP/(TP + FP)$, and the recall rate is $TP/(TP + FN)$, where TP is the number of true positives (discovered isoforms that are also in the annotation), FP is the number of false positives (discovered isoforms that are not in the annotation), and FN is the number of false negatives (undiscovered isoforms that are in the annotation and have every exon observed). For each group of n-subexon genes, we calculated their average precision and recall rates as presented in Fig. 2*A*. The results show that SLIDE maintains high precision rates (>80%) and good recall rates (>60%) in all groups of genes. In particular, for genes with three and four subexons, the precision and recall rates are greater than 98% and 92%, respectively. As n increases, the precision and recall rates decrease, and the variance between different simulation runs increases. This observation is reasonable because with the increase of n, the number of possible isoforms increases exponentially, as does the difficulty of isoform discovery.

To illustrate the abundance estimation accuracy of SLIDE, we applied it to 317 multi-isoform genes on chr3R in the UCSC

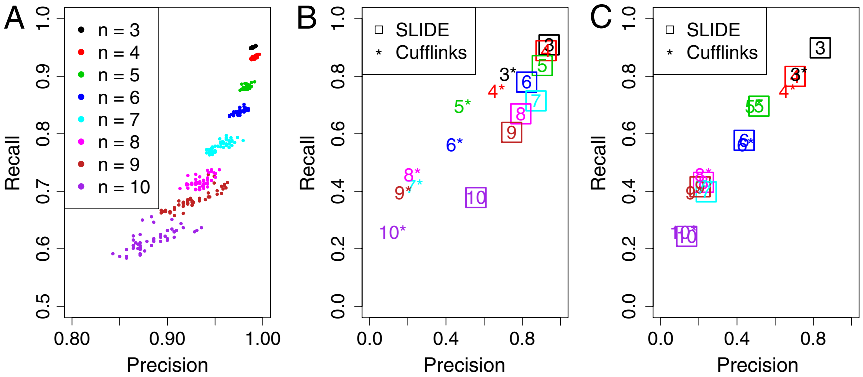

Fig. 2. Isoform discovery results. (*A*) Precision and recall rates of SLIDE on 50 simulated datasets, with different colors for groups of genes with *n* subexons ($n = 3,\cdots,10$) and every point representing the average precision and recall rates of every group on one dataset. (*B*) Precision and recall rates of SLIDE (using annotated genes/exons) and Cufflinks on dataset 1. Numbers, group indices of genes (i.e., numbers of subexons); squares/stars, SLIDE/Cufflinks results. (*C*) Precision and recall rates of SLIDE (using Cufflinks assembled genes/exons) and Cufflinks on dataset 1.

annotation (798 isoforms in total), with the same simulated paired-end reads. From reads of each simulation run, SLIDE estimates the 798 isoform proportions normalized by each gene. We calculated the Pearson correlation between the estimates and the true isoform proportions used in the simulation, and we found that the correlation coefficients of the 50 runs range from 0.92 to 0.95. We also illustrate the abundance estimation accuracy of SLIDE by a scatter plot of the median estimated isoform proportions over the 50 runs vs. true isoform proportions in Fig. 3*A* ($R = 0.99$).

This simulation study shows satisfactory performance of SLIDE in isoform discovery and abundance estimation. Further simulation studies with lowly expressed genes are in *SI Text*.

mRNA Isoform Discovery on modENCODE Data. The main feature of SLIDE is discovery of mRNA isoforms from RNA-Seq data. Four modENCODE (6) *D. melanogaster* RNA-Seq datasets (Table 1) are used in the real data analysis. Again, for illustration purposes, we focus on the 1,972 genes with 3–10 subexons on chr3R of *D. melanogaster*. To avoid the effects of high false positive and negative rates of RNA-Seq data in lowly expressed genes (23), we applied SLIDE to genes with RPKM (number of reads per kilobase per million of mapped reads) (10) greater than 1.

We compare SLIDE with Cufflinks (version 0.9.3) in terms of their isoform discovery precision and recall rates, evaluated by the UCSC annotation in a similar way to the simulation study (see *SI Text*). We note that SLIDE and Cufflinks target the isoform discovery problem from two different aspects. SLIDE discovers isoforms from given gene and exon structures, whereas Cufflinks contructs isoforms from its de novo assembled genes and exons. Hence, we carried out the comparison in two ways: (*i*) SLIDE with input genes and exons from the UCSC annotation vs. Cufflinks; (*ii*) SLIDE with input genes and exons assembled by Cufflinks vs. Cufflinks. The former is to evaluate the overall performance of the two methods under their default settings, whereas the latter is to specifically compare their isoform construction performance given the same set of genes and exons. The comparison results on dataset 1 (Table 1) are summarized in Fig. 2 *B* and *C*. (See *SI Text* for results on other datasets.)

Fig. 2*B*, corresponding to the first comparison, shows that SLIDE with input genes and exons from the annotation has significantly higher precision and recall rates than Cufflinks'. In the second comparison, with de novo genes and exons assembled by Cufflinks, SLIDE has better precision and recall rates than Cufflinks has for genes with three and four subexons, and for the rest of genes, the two methods have similar performance (Fig. 2*C*). We observe that the overall precision and recall rates in Fig. 2*C* are worse than those of SLIDE in Fig. 2*B*. These results remind us of the concerns voiced by other researchers about constructing isoforms based on de novo genes and exons built solely from RNA-Seq data (7, 8). We speculate that results of the second comparison are not enough to illustrate the isoform construction performance of SLIDE and Cufflinks, because the similarly low precision and recall rates observed in Fig. 2*C* might have been dominated by the disagreement between the de novo assembled genes/exons and the annotation. Hence, we performed an additional comparison on a smaller set of 246 genes whose de novo exons assembled by Cufflinks agree with the annotation. This comparison provides a direct evalulation on the isoform construction performance of SLIDE and Cufflinks. We found that isoforms discovered by SLIDE have an average precision rate of 93% and a recall rate of 96%, both higher than the average precision rate (89%) and recall rate (94%) of isoforms found by Cufflinks. This result demonstrates that SLIDE has higher acurracy than Cufflinks has in isoform construction from a given set of genes and exons. For more details, see *SI Text*.

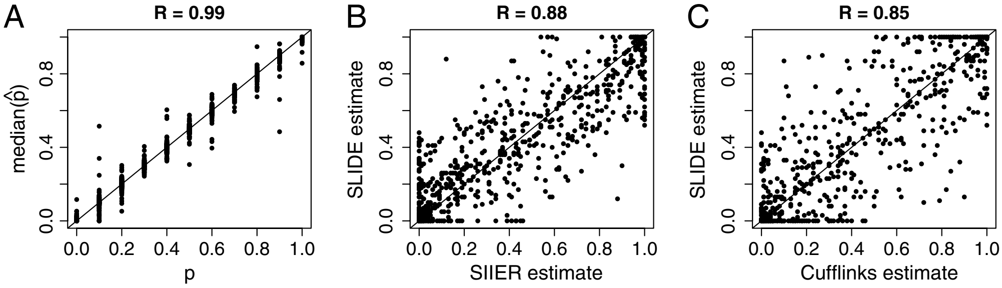

Fig. 3. Abundance estimation results. (*A*) *p* vs. median ($\hat{p}$) of 798 isoforms on 50 simulated datasets. *p*, true isoform proportion; median ($\hat{p}$), median of the 50 estimated isoform proportions. (*B*) SLIDE vs. SIIER estimates of the 798 isoforms on dataset 1. (*C*) SLIDE vs. Cufflinks estimates of the 798 isoforms on dataset 1.

Table 1. modENCODE datasets used in the analysis

Dataset	Type	Sample	Read length	Total number of reads	Sequence Read Archive (http://www.ncbi.nlm.nih.gov/sra) numbers
1	paired-end	ML-DmBG3-c2	37 bp	25,094,224	SRX003838, SRX003839
2	paired-end	Kc167	37 bp	18,602,220	SRX003836, SRX003837
3	paired-end	Kc167	76 bp	20,118,748	SRR070261, SRR070269, SRR111873
4	paired-end and single-end	embryo 16-17h	76 bp	23,388,810 and 27,913,445	SRR023600, SRR035402, SRR023720, SRR023715, SRR023751, SRR023707, SRR023826

By a detailed inspection of the isoforms discovered by Cufflinks, we find that many discovered isoforms are fragments of annotated isoforms in public databases. This is mainly due to the difficulty in de novo construction of gene boundaries. Cufflinks also has troubles in detecting lowly expressed genes de novo. By contrast, SLIDE can discover correct isoforms even with a small number of reads, based on existing gene boundary information. For instance, when applied to dataset 1, SLIDE has discovered isoforms in 1,084 genes (RPKM > 1) out of the total 1,972 genes, whereas Cufflinks has only found isoforms in 801 genes. These observations confirm again the importance of having correct gene boundaries in isoform discovery. Another advantage of SLIDE is the usage of a stochastic approach to simultaneously detect isoforms with alternative starts/ends [e.g., (1,2,3,4) and (2,3,4)], where Cufflinks will only discover the longest one (1). However, when there are significant RNA-Seq data biases in 5′ and 3′ ends of mRNA transcripts, the deterministic approach of Cufflinks may be more robust. In the future, with the continuing development of sequencing technology and promising improvement in RNA-Seq signal-to-noise ratios, we would expect the stochastic approach of SLIDE to be preferred.

There are other isoform discovery methods that use sparse estimation but with different methodology (15, 24). A numerical comparison between SLIDE and IsoLasso (15) shows that SLIDE has higher accuracy in isoform discovery. For detailed comparison information, please see *SI Text*.

mRNA Isoform Abundance Estimation on modENCODE Data. Another feature of SLIDE is to estimate the abundance of mRNA isoforms discovered or other specified (e.g., annotated) from an RNA-Seq sample. Because of the lack of ground truth of isoform abundance in datasets 1–4 (Table 1), to evaluate the abundance estimation performance of SLIDE, we compare its estimates to those of two popular methods: statistical inferences for isoform expression in RNA-Seq (SIIER) (12) and Cufflinks (1). Note that SLIDE returns estimates of mRNA isoform proportions that are equivalent and convertible to the common abundance measure, isoform RPKMs (10) used in SIIER.

In the comparison between SLIDE and SIIER, both methods estimate the isoform abundance of the 317 chr3R genes with multiple isoforms in the UCSC annotation. In dataset 1, after removing 25 genes with high expression variance among exons (see *SI Text*), we obtain a scatter plot of the two sets of estimates in Fig. 3*B* ($R = 0.88$). A similar comparison is carried out between SLIDE and Cufflinks, and the results are in Fig. 3*C* ($R = 0.85$). The results show that SLIDE obtains estimates similar to those of SIIER and Cufflinks. For more discussions on the results, see *SI Text*.

Miscellaneous Effects on Isoform Discovery. Using datasets 1–4 (Table 1), we study the following critical issues affecting isoform discovery from RNA-Seq data.

1. GC content variation. To study the usefulness of considering GC content variation in isoform discovery, we additionally implemented another version of **F**, assuming the cDNA fragment starting position s_1 as uniform across all subexons. Note that our default **F** assumes the density of s_1 as uniform within subexons but proportional to GC content between subexons, as motivated by observed high correlation between read coverage and GC content variation (2, 4) (see *SI Text*). Isoform discovery results on dataset 1 by SLIDE based on the two version of **F** are compared in Table 2. Recall rates are similar in both results, but precision rates are improved with the consideration of GC content. These results indicate that GC content can provide SLIDE with useful information in modeling **F**, and thus support various attempts of using GC content information to correct RNA-Seq data noise (3, 4).
2. Read/fragment length effects. To explore the effects of RNA-Seq read lengths on isoform discovery, we applied SLIDE to datasets 2 and 3. The two datasets are generated from the same Kc167 sample of similar sequencing depth but with different read lengths: 37 bp (dataset 2) vs. 76 bp (dataset 3). We compare the isoform discovery results on both datasets in Fig. 4*A*. The precision and recall rates for genes with 3–9 subexons are surprisingly higher with the 37-bp data than the 76-bp data. This result contradicts our expectation that RNA-Seq data with longer read length would provide more information on exon junctions that are crucial to isoform discovery. Trying to find a plausible explanation, we checked the empirical distribution of cDNA fragment lengths in single-exon genes for both data, and found the distribution close to $N(166,26^2)$ and $N(127,13^2)$ for the 37-bp and 76-bp data, respectively. The fact that the 37-bp data contain more long fragments is a result of different experimental protocols, and is likely to be a reason for the observed unexpected comparison results. A simulation study with different read and fragment lengths reveals that the fragment length distribution has larger effects than the read length has on isoform discovery, and to some extent confirms our real data observation (see *SI Text*).
3. Paired-end vs. single-end RNA-Seq data. Compared with single-end RNA-Seq data, the more recent paired-end data provides more information on exon junctions and thus is expected to return isoform discovery results with higher precision rates. But if both single-end and paired-end data are available for the same RNA-Seq sample, the former can possibly complement the latter by providing more exon expression information, helping capture lowly expressed exons in rare

Table 2. Comparison of isoform discovery results by SLIDE with two versions of F

n		3	4	5	6	7	8	9	10
without GC	precision	0.93	0.90	0.87	0.80	0.83	0.75	0.71	0.49
	recall	0.91	0.89	0.83	0.77	0.71	0.68	0.61	0.36
with GC	precision	0.94	0.92	0.90	0.82	0.87	0.79	0.74	0.56
	recall	0.91	0.89	0.84	0.78	0.71	0.67	0.60	0.38

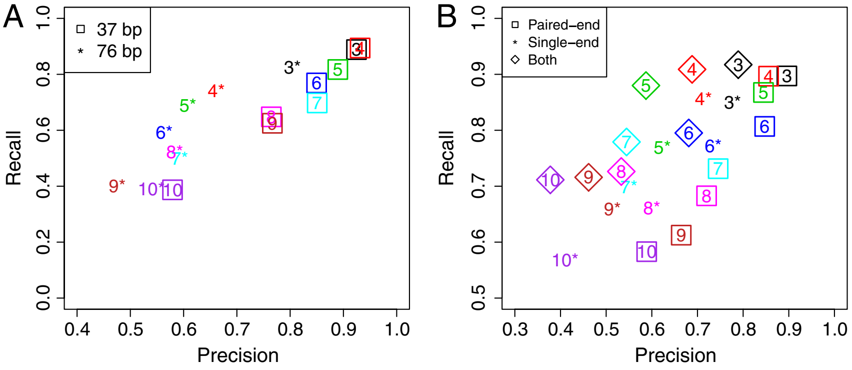

Fig. 4. Miscellaneous effects. (*A*) Precision and recall rates of SLIDE on 37 bp and 76 bp paired-end RNA-Seq data (datasets 2–3). (*B*) Precision and recall rates of SLIDE on dataset 4 with paired-end data only (squares), single-end data only (stars), and both (diamonds).

isoforms, and thus resulting in isoform discovery results with higher recall rates. Because SLIDE has the flexibility of inputting both single-end and paired-end RNA-Seq data (see *Methods*), we tested these hypotheses by applying it to dataset 4, which has both single-end and paired-end data from the same sample and of similar numbers of reads (Table 1). We specifically compare the results of SLIDE on (*i*) paired-end data, (*ii*) single-end data, and (*iii*) both paired-end and single-end data in Fig. 4*B*. From the figure, we observe that using paired-end data alone has the highest precision rates for all the genes, whereas using both data has the best recall rates. These results confirm our intuitive hypotheses that paired-end data alone gives more precise information than single-end data does in isoform discovery; however, single-end data does provide extra exon expression information as well as noise when it is used in addition to paired-end data, hence resulting in higher recall rates and lower precision rates.

Discussion

We have proposed a sparse linear model approach (SLIDE) capable of discovering mRNA isoforms of given genes and estimating the abundance of discovered or other specified isoforms from RNA-Seq data. Compared to existing approaches (1, 12), SLIDE (*i*) discovers isoforms from all possible ones based on known gene and exon boundaries (e.g., from the UCSC annotation), (*ii*) uses a stochastic approach with a quantitatively modeled design matrix **F** (i.e., conditional probabilities of observing RNA-Seq reads from mRNA isoforms) in isoform discovery, (*iii*) uses the same linear model subsequently for abundance estimation on discovered or other specified isoforms, and (*iv*) can be used as a downstream isoform discovery tool of de novo gene and exon assembly algorithms. Other widely used isoform discovery methods (1, 20) find isoforms based on their own de novo genes and exons solely assembled from RNA-Seq reads, and thus their discovered isoforms are highly dependent on the accuracy of de novo assembly. SLIDE can avoid possible de novo assembly errors (2) by using known gene and exon boundaries; it can also integrate de novo assemblies with known ones to prevent the risk of missing isoforms involving novel exons. SLIDE will also benefit from ongoing efforts of improving *D. melanogaster* transcriptome annotations (6).

We have also explored various factors that may affect the performance of SLIDE on isoform discovery. Our results suggest that (*i*) the consideration of GC content variation in modeling **F** can improve the precision, (*ii*) the cDNA fragment size selection protocol and the resulting cDNA fragment lengths have larger effects than read lengths have on both the precision and recall, and (*iii*) paired-end RNA-Seq data provides more accurate information than single-end data does in isoform discovery, but the addition of single-end data would help with the discovery of rare isoforms.

As demonstrated by the isoform discovery and abundance estimation results, SLIDE shows great promise as a tool for handling the two tasks sequentially with a shared linear model. The modeled design matrix **F** is also shown to be a good quantitative representation of sampling RNA-Seq reads from mRNA isoforms, in contrast to the binary representation used in other isoform discovery methods (1, 11, 15, 20). We still lack the information to model irregular systematic RNA-Seq biases, such as low read coverage in transcript ends and significant read coverage variation unexplained by GC content. But we expect SLIDE to have increased power when such modeling becomes possible with the standardization of RNA-Seq protocols and the improvement of technology. Finally, SLIDE can be easily extended to incorporate mRNA isoform information from EST (21), CAGE (19), and RACE (18) data in addition to RNA-Seq data to refine its linear model and obtain more accurate isoform discovery results.

Methods

Linear Model Formulation and Identifiability Issue. In the linear modeling of paired-end RNA-Seq data, we first categorize reads into paired-end bins. For an n-subexon gene, possible paired-end bins are $\{(i,j,k,l), 1 \le i \le j \le k \le l \le n\}$, whose total number is $m_p = n + 3\binom{n}{2}1_{(n\ge2)} + 3\binom{n}{3}1_{(n\ge3)} + \binom{n}{4}1_{(n\ge4)}$. Then RNA-Seq data is transformed into bin counts (i.e., number of reads in each bin), which are further normalized as bin proportions **b**. Second, we enumerate all the possible isoforms of an n-subexon gene as $I_1,\cdots,I_{2^n-1}$, and denote **p** as the isoform proportions to be estimated. Third, we relate unknown **p** to observed **b** by a design matrix **F**, where $F_{jk} = \Pr(j\text{th bin}|k\text{th isoform})$ (i.e., the conditional probability of observing reads in the jth bin given that the reads are from the kth isoform). (See next section for the modeling of **F**). Then, we write the following linear model:

$$b_j = \sum_{k=1}^{2^n-1} F_{jk}p_k + \epsilon_j, \qquad j = 1,\cdots,m_p, \quad \text{or} \quad \mathbf{b} = \mathbf{F}\mathbf{p} + \epsilon, \qquad [2]$$

where $\epsilon = (\epsilon_1,\cdots,\epsilon_{m_p})$ is the random noise whose components are independent and have mean 0.

We note that the linear model (Eq. **2**) becomes unidentifiable when $m_p < 2^n - 1$ or equivalently $n \ge 9$. The model may also be unidentifiable when $n < 9$ due to possible collinearity of **F**. To solve this identifiability issue, we reduced the number of parameters dim(**p**) by adding a preselection procedure on isoforms. Also, given observed false zero bin counts of certain junction reads, we applied a preselection procedure on observations, too. (See *SI Text* for details.) We write the postselection linear model as

$$b_j = \sum_{k=1}^{K} F_{jk}p_k + \epsilon_j, \qquad j = 1,\cdots,J. \qquad [3]$$

We note that the unidentifiability issue still exists in many genes even after the preselection procedures, so sparse estimation is necessary (see *SI Text*).

For single-end data and the combination of both single and paired-end data, we can derive a similar linear model (see *SI Text*).

Modeling of Conditional Probability Matrix. Modeling of the conditional probability matrix $\mathbf{F} = (F_{jk})$, $1 \le j \le J$, $1 \le k \le K$ is a key part in the estimation of $\mathbf{p}$ (Eq. **3**). In paired-end RNA-Seq data, a mate pair represents ends of a cDNA fragment reversely transcribed from an mRNA transcript. In this sense, F_{jk} is the conditional probability that cDNA fragments with ends in the jth bin are reversely transcribed from mRNA transcripts in the kth isoform. With this interpretation, we model $\mathbf{F}$ with the following three assumptions.

1. The density of a cDNA fragment's starting position (or the density of s_1 in Fig. 1), denoted by f, is uniform within subexons but proportional to GC content between subexons in an mRNA transcript.
2. The cDNA fragment length ($\ell = e_2 - s_1$ in Fig. 1) distribution is modeled as truncated Exponential with density denoted by g. This modeling choice is based on empirical observations and Poisson point process approximations (see *SI Text*). SLIDE can also easily take other reasonable fragment length distributions.
3. Starting positions and fragment lengths are assumed to be independent.

In a two-subexon gene example (Fig. 1), suppose that the two subexons have boundaries $[a_1,b_1]$ and $[a_2,b_2]$. Then, reads in bin $j = (1,1,2,2)$ have $s_1 \in [a_1, b_1 - r + 1]$ and $e_2 \in [a_2 + r - 1, b_2]$. For $k = (1,2)$, we calculate $F_{jk} = \int_{a_1}^{b_1-r+1} f(s_1)(\int_{a_2+r-1-s_1}^{b_2-s_1} g(\ell)d\ell)ds_1$.

For single-end data and the combination of both single and paired-end data, $\mathbf{F}$ can be similarly calculated (see *SI Text*).

mRNA Isoform Discovery. In isoform discovery, we expect sparse parameter estimation from the linear model (Eq. **3**), because the number of mRNA isoforms for most *D. melanogaster* genes is below four (17) and far less than the number of possible isoforms K. L_1 penalization approach is widely used for sparse estimation and has applications in high-dimensional and potentially sparse biological data (25). We also observe that annotated isoforms often contain a large proportion of subexons, and thus expect isoform candidates with more subexons to be more likely true. Hence, we add an L_1 penalty term in the objective function below to limit the number of discovered isoforms as well as to favor the "longer isoforms":

$$\hat{\mathbf{p}} = \mathrm{argmin}_{p_1,\ldots,p_K \ge 0} \sum_{j=1}^{J} (b_j - \mathbf{F}_j \mathbf{p})^2 + \lambda \sum_{k=1}^{K} \frac{|p_k|}{n_k}, \qquad [4]$$

where n_k is the number of subexons in the kth isoform and $\mathbf{F}_j$ is the jth row of $\mathbf{F}$. With n_k in the penalty term, p_k would thus be favored if n_k is large. We note that this is a variant of Lasso, a regularization regression method for cases in which the number of parameters to be estimated exceeds the number of observations and most of the parameters are expected to be zeros (22). The difference between our penalty term and the one in standard Lasso is that the latter only aims to limit the number of discovered isoforms without favoring longer ones. Discussions about choosing L_1 over L_0 regularization and using different likelihoods in the linear model are in *SI Text*.

Table 3. $\lambda^{(n)}$ selection results for different datasets

n	3	4	5	6	7	8	9	10
Datasets 1–2 (37 bp)	0.3	0.3	0.3	0.4	0.4	0.4	0.4	0.5
Datasets 3–4 (76 bp)	0.2	0.2	0.2	0.4	0.3	0.4	0.3	0.3
Simulation data (37 bp)	0.3	0.3	0.3	0.4	0.4	0.4	0.4	0.5

16 candidate λs: 10^{-6}, 10^{-4}, 10^{-3}, 0.01, 0.04, 0.07, 0.1, 0.2, 0.3, 0.4, 0.5, 0.6, 0.7, 0.8, 0.9, 1

The selection of the regularization parameter λ (Eq. **4**) is by a stability criterion that aims to return the most stable results over different runs of estimation (26). Because low signal-to-noise ratios in lowly expressed genes may significantly bias the λ selection and genes of the same number of subexons have similar dim($\mathbf{p}$) and dim($\mathbf{b}$) in Eq. **4**, we group genes by their numbers of subexons n and select an optimal $\lambda^{(n)}$ for each group from 16 candidate values $(\lambda_i)_{i=1}^{16}$ (see Table 3). The selection procedure is described in *SI Text*, and the chosen $\lambda^{(n)}$ values for datasets 1–4 and the simulation data are in Table 3.

R package "penalized" (27) is used in the implementation.

mRNA Isoform Abundance Estimation. The SLIDE linear model (Eq. **3**) can also be used for abundance estimation of discovered or other specified (e.g., annotated) isoform proportions. Because the number of discovered or annotated isoforms is smaller than the number of bin proportions, the linear model is identifiable. Thus, we use nonnegative least squares without a penalty term to estimate the isoform proportions. R package "NNLS" is used in the implementation (28).

ACKNOWLEDGMENTS. We thank Qunhua Li and Nathan Boley in Department of Statistics, University of California, Berkeley, for their insightful comments during discussions. This work is supported in part by Grants HG004695, HG005639, and EY019094 from the National Institutes of Health. We would like to thank the Statistical and Applied Mathematical Sciences Institute for providing great research environments to C.-R.J. to continue participating in this project.

1. Trapnell C, et al. (2010) Transcript assembly and quantification by RNA-Seq reveals unannotated transcripts and isoform switching during cell differentiation. *Nat Biotechnol* 28:511–515.
2. Dohm JC, Lottaz C, Borodina T, Himmelbauer H (2010) Substantial biases in ultra-short read data sets from high-throughput DNA sequencing. *Nucleic Acids Res* 36:e105.
3. Hansen KD, Brenner SE, Dudoit S (2010) Biases in Illumina transcriptome sequencing caused by random hexamer priming. *Nucleic Acids Res* 38:e131.
4. Li J, Jiang H, Wong WH (2010) Modeling non-uniformity in short-read rates in RNA-Seq data. *Genome Biol* 11:R50.
5. Roberts A, Trapnell C, Donaghey J, Rinn JL, Pachter L (2011) Improving RNA-Seq expression estimates by correcting for fragment bias. *Genome Biol* 12:R22.
6. modENCODE Consortium (2009) Unlocking the secrets of the genome. *Nature* 459:927–930.
7. modENCODE Consortium (2010) Identification of functional elements and regulatory circuits by *Drosophila* modENCODE. *Science* 330:1787–1797.
8. Gerstein MB, et al. (2010) Integrative analysis of the *Caenorhabditis elegans* genome by the modENCODE project. *Science* 330:1775–1787.
9. Lee S, et al. (2011) Accurate quantification of transcriptome from RNA-Seq data by effective length normalization. *Nucleic Acids Res* 39:e9.
10. Mortazavi A, Williams BA, McCue K, Schaeffer L, Wold B (2008) Mapping and quantifying mammalian transcriptomes by RNA-Seq. *Nat Methods* 5:621–628.
11. Feng J, et al. (2010) Inference of isoforms from short sequence reads. *14th Annual International Conference on Research in Computational Molecular Biology (RECOMB 2010), Lecture Notes on Computer Science*, 6044 (Springer, Berlin/Heidelber), pp 138–157.
12. Jiang H, Wong WH (2009) Statistical inferences for isoform expression in RNA-Seq. *Bioinformatics* 25:1026–1032.
13. Li B, Ruotti V, Stewart RM, Thomson JA, Dewey CN (2010) RNA-Seq gene expression estimation with read mapping uncertainty. *Bioinformatics* 26:493–500.
14. Richard H, et al. (2011) Prediction of alternative isoforms from exon expression levels in RNA-Seq experiments. *Nucleic Acids Res* 38:e112.
15. Li W, Feng J, Jiang T (2011) IsoLasso: A LASSO regression approach to RNA-Seq based transcriptome assembly. *15th Annual International Conference on Research in Computational Molecular Biology (RECOMB 2011), Lecture Notes on Computer Science*, 6577 (Springer, Berlin/Heidelber), pp 168–188.
16. Flicek P, et al. (2011) Ensembl 2011. *Nucleic Acids Res* 39(Suppl 1):D800–D806.
17. Fujita PA (2011) The UCSC Genome Browser database: Update 2011. *Nucleic Acids Res* 39(Suppl 1):D876–D882.
18. Frohman MA, Dush MK, Martin GR (1988) Rapid production of full-length cDNAs from rare transcripts: Amplification using a single gene-specific oligonucleotide primer. *Proc Natl Acad Sci USA* 85:8998–9002.
19. Shiraki T, et al. (2003) Cap analysis gene expression for high-throughput analysis of transcriptional starting point and identification of promoter usage. *Proc Natl Acad Sci USA* 100:15776–15781.
20. Guttman M, et al. (2010) Ab initio reconstruction of cell typespecific transcriptomes in mouse reveals the conserved multi-exonic structure of lincRNAs. *Nat Biotechnol* 28:503–510.
21. Adams MD, et al. (2003) Complementary DNA sequencing: Expressed sequence tags and human genome project. *Science* 252:1651–1656.
22. Tibshirani R (1996) Regression shrinkage and selection via the lasso. *J R Stat Soc Series B Stat Methodol* 58:267–288.
23. Liu S, Lin L, Jiang P, Wang D, Xing Y (2011) A comparison of RNA-Seq and high-density exon array for detecting differential gene expression between closely related species. *Nucleic Acids Res* 39:578–588.
24. Xia Z, Wen J, Chang C, Zhou X (2011) NSMAP: A method for spliced isoforms identification and quantification from RNA-Seq. *BMC Bioinformatics* 12:162.
25. Meinshausen N, Bühlmann P (2010) Stability selection. *J R Stat Soc Series B Stat Methodol* 72:417–473.
26. Dahinden C, Parmigiani G, Emerick MC, Bhlmann P (2007) Penalized likelihood for sparse contingency tables with an application to full-length cDNA libraries. *BMC Bioinformatics* 8:1–11.
27. Goeman JJ (2010) Penalized: L1 (Lasso) and L2 (Ridge) penalized estimation in GLMs and in the Cox model. R package version 0.9-31., Available at http://cran.r-project.org/web/packages/penalized/.
28. Mullen KM, van Stokkum IHM (2010) nnls: The Lawson-Hanson algorithm for non-negative least squares (NNLS). R package version 1.3., Available at http://cran.r-project.org/web/packages/nnls/.

Supporting Information

Li et al. 10.1073/pnas.1113972108

SI Text

1. Linear Modeling of RNA-Seq Data. Linear modeling of paired-end RNA-Seq data has been discussed in *Methods* of the main paper. The main points include (*i*) the definition of paired-end bins to summarize the key information in RNA-Seq data for isoform discovery, (*ii*) the enumeration of all possible isoforms from defined subexons, (*iii*) the modeling of conditional probabilities of observing reads in different bins given an isoform, and (*iv*) the construction of a linear model to estimate isoform proportions from observed bin counts.

Below, we present more details about modeling the fragment length distribution in **F** and construction of linear model for single-end data.

1.1. The fragment length distribution. Modeling the cDNA fragment length distribution is a key part in constructing the design matrix **F** of the linear model. Truncated Exponential is a reasonable candidate for the distribution, based on a Poisson point process assumption on a fragment's 3′ end with the 5′ end fixed and a size selection step in RNA-Seq protocols. Another widely used candidate in existing RNA-Seq tools is Normal distribution (1). To evaluate the two distributions, we compared them with empirical distributions of cDNA fragment lengths in paired-end RNA-Seq data. However, actual fragment lengths are unknown in genes exhibiting alternative splicing events, thus posing difficulties in obtaining the empirical distributions. To tackle this problem, a conservative solution is to calculate an empirical length distribution of cDNA fragments with both ends in the same subexon where no alternative splicing occurs. The good side of this solution is that the fragment lengths used in the calculation are actual, but the downside is that some long fragments across exons are not considered. Another solution is to calculate an empirical length distribution based on cDNA fragments in genes with no alternative splicing events in the UCSC *Drosophila melanogaster* (September 2010) annotation (16). This solution has the advantage of observing all sorts of fragment lengths, but its disadvantage is that wrong fragment lengths may be used if the annotation is incomplete. We employed both solutions to calculate the emprical distributions from dataset 1, and plotted them against either truncated Exponential or Normal distribution in Q-Q plots (Fig. S1). Parameters in the truncated Exponential and Normal distributions are chosen in such a way that both distributions have the same mean and variance as in the empirical distribution. Q-Q plots in Fig. S1 show that both truncated Exponential and Normal distributions are reasonable approximations of the fragment length distribution.

1.2. Linear modeling of single-end RNA-Seq data. For single-end RNA-Seq data, we can derive a similar linear model to the one used for paired-end data (Eq. **3** in the main paper). First, we enumerate possible isoforms in the same way as for the paired-end data, and categorize reads into single-end bins, defined as two-dimensional vectors indicating subexon indices of the reads. For example, single-end bin (i, j) contains reads whose 5′ and 3′ ends are in subexon i and j, respectively. A single-end bin count is defined as the number of reads in that bin. Bin counts of every gene are normalized as bin proportions, denoted by **b**. Second, we construct a linear model to estimate isoform proportions **p** from observed single-end bin proportions, with a design matrix **F** as the conditional probabilies of observing reads in different single-end bins given an isoform. The modeling and calculation of the conditional probabilities for single-end data are similar to those for paired-end data in the main paper. We consider a single-end bin as equivalent to a combination of multiple paired-end bins. For example, in a two-subexon gene, reads in single-end bin (1,1) correspond to paired-end reads in bins (1,1,1,1), (1,1,1,2), and (1,1,2,2). So the conditional probability of observing reads in single-end bin (1,1) given an isoform equals to the sum of conditional probabilities of observing reads in each of the three paired-end bins given the same isoform. In general, we calculate the conditional probability of observing reads in single-end bin j given isoform k as $\sum_{r\in S_j} F'_{rk}$, where S_j is the set of paired-end bins corresponding to the single-end bin j, and F'_{rk} is the conditional probability for paired-end data whose calculation has been described in details in the main paper. Last, we write a linear model in the same formula as in Eq. **3** of the main paper.

For combined paired-end and single-end data, we can simply construct a linear model by catenating the observation vectors and combining the design matrices by rows in the linear models for paired-end and single-end data, respectively. Hence, the linear model used in SLIDE (sparse linear modeling of RNA-Seq data for isoform discovery and abundance estimation) can accomodate for different types of RNA-Seq data: paired-end, single-end, or both.

1.3. Identifiability and preselection procedures. To avoid the unidentifiability issue due to collinearity in the linear model (Eq. **2** in the main paper), we applied a preselection procedure: Only isoforms whose all subexon junctions have been observed are selected as candidates; for genes with more than two subexons, single-subexon isoforms are excluded from the candidates because of their rare existence. With this procedure, the number of parameters for an n-subexon gene can be reduced from $2^n - 1$ to a significantly smaller number.

About the observations, there are frequently false zero counts of junction-end bins. We define junction-end bins as bins that include paired-end reads with at least one end across exon junctions [e.g., junction-end bins (1,1,1,2) and (1,2,2,2) include paired-end reads with one end covering the junction between subexons 1 and 2, whereas bin (1,1,2,2) is not a junction-end bin]. When bin (1,1,2,2) has positive counts, the expected counts of bins (1,1,1,2) and (1,2,2,2) should be positive, too; however, due to the difficulty of mapping junction reads, junction-end bins (1,1,1,2) and (1,2,2,2) are often observed with false zero counts. Thus, we exclude false zero junction-end bin proportions from the observations.

As an illustration of the effects of such preselection procedures, we calculate the numbers of genes with unidentifiability issues in their linear models (i.e., rank(**F**) $< K$ in Eq. **1** of the main paper) before and after the preselection procedures for every group of n-subexon genes ($n = 3,\ldots,10$). The numbers are summarized in Table S1, which shows that the preselection procedures have effectively overcome the unidentifiability issue for genes with three subexons and alleviated the problem for a few genes with more subexons. However, the percentage of genes with unidentifiablity issues remains high after the preselection procedure for genes with more than three subexons; we see that the sparse estimation in SLIDE is still necessary.

1.4. L_1 vs. L_0 regularization. In sparse estimation, L_1 penalty in Lasso is linear and ensures convexity of the objective function (Eq. **4** in the main paper). It also has the convexity property in logistic and Poisson regressions. Lasso does variable selection and shrinkage, thus permitting isoform discovery in SLIDE. L_0

penalty is also a possible choice for sparse estimation. It was reported that L_0 penalty can lead to a sparser model when the number of variables (e.g., the number of isoform candidates) is far larger than the number of relevant variables (e.g., the number of existing isoforms), whereas L_1 penalty in Lasso has to use a large λ to screen out spurious variables and causes biases in retained variables (2, 3). However, L_0 regularization is computationally disadvantageous because it makes the optimization problem nonconvex, and it has been shown that L_1 is a good surrogate for L_0 in many cases. In computational biology, L_1 regularization is shown to be a good approach for high-dimensional and potentially sparse data (4). In our case, SLIDE does isoform discovery and abundance estimation in two steps, so the biased estimates of isoforms in the discovery step would not affect the subsequent abundance estimation step as long as true isoform estimates are not shrunk to zeros by Lasso. This is different from IsoLasso and NSMAP, which use one-step sparse estimation for simultaneous isoform discovery and abundance estimation (5, 6). Moreover, in our estimation, the existence of n_k (the number of exons in the kth isoform) in the penalty term would reduce the difference between L_1 and L_0 regularization. Therefore, L_1 regularization is a reasonable choice for our sparse estimation.

1.5. Selection of the regularization parameter in sparse estimation. The selection of the regularization parameter λ (Eq. **4** in the main paper) is by a stability criterion that aims to return the most stable results over different runs of estimation (7). Because genes of the same number of subexons have similar dim($\mathbf{p}$) and dim($\mathbf{b}$) in Eq. **4** of the main paper, we decided to group genes by their numbers of subexons n and select an optimal $\lambda^{(n)}$ for each group from 16 candidate values $(\lambda_i)_{i=1}^{16}$ (see Table 3 of the main paper). This grouping is particularly advantageous for selecting λ for lowly expressed genes, whose signal-to-noise ratios are low. Highly expressed gene signals can counteract the noise in the lowly expressed genes of the same group.

Suppose that there are $m^{(n)}$ genes with n subexons, $n = 3,\cdots,10$. The selection procedures following the stability criterion are as follows.

1. For the rth gene with n subexons, $r = 1,\cdots,m^{(n)}$, use $\lambda = \lambda_i$, $i = 1,\cdots,16$ in Eq. **4** to estimate $\hat{\mathbf{p}}$ for 50 runs. In each run, use randomly sampled one half of the reads in the gene as input into SLIDE. Define q_{irk} as the proportion of runs in which $\hat{p}_k > 0$. Define $\bar{q}_{ir} = \frac{\sum_{k=1}^{K} q_{irk}}{\sum_{k=1}^{K} I(\hat{p}_k>0 \text{ in some runs})}$.
2. Calculate the average of $\bar{q}_{ir}$ over the $m^{(n)}$ genes as $\tilde{q}_i = \frac{1}{m^{(n)}} \sum_{r=1}^{m^{(n)}} \bar{q}_{ir}$.
3. Choose $\lambda^{(n)}$ as λ_{i^*}, where $i^* = \text{argmax}_i \tilde{q}_i$.

The selected $\lambda^{(n)}$ for datasets 1–4 and the simulation data are in Table 3 of the main paper.

2. More Simulation Studies. ***2.1. Simulation studies with different read coverages.*** To study the isoform discovery accuracy of SLIDE in lowly expressed genes, we did a simulation study with three different read coverages: (*i*) 10 reads per kilobase of an annotated gene, (*ii*) 50 reads per kilobase of an annotated gene, and (*iii*) 100 reads per kilobase of an annotated gene. The simulated reads are paired-end with 37-bp length in each end. Precision and recall rates of SLIDE using the simulated data are summarized in Fig. S2, which shows that SLIDE has improved isoform discovery accuracy as the read coverage increases, as we expected. The improvement is significant when the read coverage increases from 10 reads per kilobase to 50 reads per kilobase, and the improvement becomes less significant when the read coverage increases further to 100 reads per kilobase. Given that many paired-end RNA-Seq data have more than 10 million reads, 10 reads per kilobase would correspond to less than 1 RPKM (number of reads per kilobase per million of mapped reads) in those data. We note that a gene with such low read coverage and multiple exons is not likely to have all its exon junctions covered by reads, thus posing great difficulties on isoform discovery. As illustrated by this simulation study, SLIDE is robust to changes in gene expression levels when read coverage is beyond a certain threshold, and SLIDE has higher precision and recall rates and lower estimation variance as read coverage increases. When gene expression is too low (e.g., 10 reads per kilobase), some exons or exon junctions would not be observed and the dimensionality of observations in the core linear model would be reduced, thus resulting in incorrect estimation results by SLIDE. At the read coverage of 10 reads per kilobase, we have tried other likelihoods (multinomial and Poisson) to model the responses (i.e., bin counts) in the linear model of SLIDE, but the precision and recall rates are similarly low (see subsection 2.2). [Please note that our Poisson regression has a similar objective function as the maximum-likelihood approach used in NAMAP (6) has in the optimization, except for differences in the design matrix and penalty term.] This missing data problem associated with lowly expressed genes is not unique to SLIDE, because to accurately recover missing reads from observed data remains a big challenge for current RNA-Seq isoform discovery and quantification methods. Because of data noise and biases introduced at many experimental steps of the current RNA-Seq protocol, it would be difficult to recover missing exons or junctions by statistical models.

2.2. Simulation studies with different likelihoods in the core linear model. To explore the effects of using different likelihoods in the generalized linear model of SLIDE (Eq **3** in the main paper), we tried three different likelihoods: Normal (the default), multinomial (logistic regression) and Poisson in the sparse estimation with simulated data. Reads were simulated under two read coverages, 10 and 100 reads per kilobase. Simulation settings are the same as described in the main paper. The results in Fig S3 illustrate that in general, the three different likelihoods do not give very different results in both read coverages. Looking more closely, we find that using Normal likelihood at read coverage 10 reads/kb gives slightly higher precision and recall rates for genes with 3–4 subexons, and using Logistic regression at read coverage 100 reads/kb gives lower precision rates for genes with 3–5 exons. In our SLIDE model, it is naturally to assume that the expected bin counts are linear in isoform quantities and to use an identity link function (Normal likelihood). These exploration results confirm that Normal likelihood is a reasonable choice.

2.3. Effects of isoform similarity and missing annotations on isoform discovery. Similarity between different isoforms of the same gene would pose difficulties on isoform discovery. There are some cases where the isoform deconvolution is not identifiable because of the similarity between true isoforms (8, 9). For example, when some isoforms are fragments of others in the true isoform set, there would usually be more than one possible set of isoforms that can explain the observed exon expression levels and exon junctions.

In situations that annotations have missing but truly expressed isoforms, there are two different cases. First, when missing isoforms have exons not included in annotated isoforms, although SLIDE is not designed to recover missing exons from data, it can solve this issue by using de novo exons assembled by other softwares [e.g., Cufflinks (1), Scripture (10)]. Second, when all the exons in missing isoforms are included in annotated isoforms, SLIDE can discover the missing isoforms with high accuracy, especially if every missing isoform has more than one unique splice junctions. In the difficult case where some missing isoforms are fragments of annotated isoforms and the isoform deconvolution is not identifiable, SLIDE would discover a set of longest isoforms with the highest probability among all the possible sets of isoforms. For example, we suppose that a three-exon gene has exon RPKMs 10, 20, and 10, respectively, and junction reads are observed between exons 1–2, and exons 2–3. In terms of the isoform deconvolution, there would be two possible sets of isoforms: (*i*) isoform (1,2,3) with RPKM 10 and isoform (2) with RPKM 10; or (*ii*) isoform (1,2) with RPKM 10 and isoform (2,3) with RPKM 10. In this case, SLIDE would favor the latter (set *ii*), which has a smaller penalty term. We design SLIDE to favor longer isoforms in the sparse estimation, by weighting each isoform abundance estimate with the inverse of its number of exons. This is based on our observations that most annotated isoforms contain many instead of few exons. In real data study, there are commonly observed 5′ and 3′ end biases in RNA-Seq data, that is, in our example above, even if the true isoform is (1,2,3), RNA-Seq read coverage in exons 1 and 3 is very likely to be lower than the read coverage in exon 2. To counteract the end biases in real RNA-Seq data, we allow SLIDE to favor isoforms with more exons in the sparse estimation. Therefore, SLIDE would find the longest isoform containing all the three exons unless the read coverage difference between exons 1 and 3 and exon 2 is significantly high.

We did simulation studies in the following three cases to illustrate the performance of SLIDE when annotations have missing isoforms but contain all the exons. In gene *RhoL*, there are four exons with lengths 379, 172, 286, and 204, respectively. The only annotated isoform is (1,2,3,4) that contains all four exons. In each of the following cases, we did 50 simulation runs with 500 paired-end 37-bp reads simulated in each run.

Case 1. Suppose that isoform (1,3,4) is missing in the annotation and its expression level is the same as that of isoform (1,2,3,4). We note that (1,3,4) contains a novel junction between exons 1 and 3 that is not in the annotated isoform (1,2,3,4). For all 50 runs, SLIDE correctly discovered both isoforms.

Case 2. Suppose that isoform (2,3,4) is missing in the annotation and its expression level is the same as that of isoform (1,2,3,4). We note that (2,3,4) is a fragment of the annotated isoform (1,2,3,4). For 49 out of the 50 runs, SLIDE correctly discovered both isoforms.

Case 3. Suppose that both isoforms (1,3,4) and (2,3,4) are missing in the annotation and both of their expression levels are the same as that of isoform (1,2,3,4). SLIDE correctly discovered all three isoforms in 18 runs. It missed isoform (2,3,4) in 18 runs, missed isoform (1,3,4) in 8 runs, and missed both in 6 runs.

From the results, we can see that it is more difficult to discover missing isoforms that are fragments of annotated isoforms, because SLIDE has to tackle end biases in real data. Nevertheless, these simulation results show that SLIDE has satisfactory performance in cases where annotations have missing isoforms.

3. More About mRNA Isoform Discovery on modENCODE Data. ***3.1. More about the comparison between SLIDE and Cufflinks.*** In the main paper, we carried out three comparisons between SLIDE and Cufflinks from different perspectives. First, we compare the two methods in their default settings, where SLIDE uses genes and exons from UCSC annotations and Cufflinks uses its de novo assembled genes and exons (Fig. 2*B* in the main paper). In the evaluation step, we compare discovered isoforms by each method with isoforms in UCSC annotations. We call a discovered isoform and an annotated isoform matched if they have the same number of exons and all of their exons overlap. Thus, our evaluation scheme is not sensitive to exon boundaries as long as de novo assembled exons are in the same loci as annotated exons. We agree that this comparison is not fair for Cufflinks, but the results still reveal two main problems of the Cufflinks results: (*i*) Cufflinks splits a gene into multiple parts when few junction reads are observed between certain exons; (*ii*) Cufflinks merges two genes on opposite strands if they overlap because the read strand information is not properly considered. SLIDE does not have those two problems because it uses annotated gene boundaries that are mostly accurate. In the second comparison, we applied both methods to de novo assembled genes and exons by Cufflinks (i.e., to compare the isoform assembly performance of SLIDE and Cufflinks given the same set of genes and exons) (Fig. 2*C* in the main paper). The comparison results show that SLIDE and Cufflinks have similar precision and recall rates, which are, however, much lower than the precision and recall rates SLIDE had when using annotated genes and exons. We were concerned that the precision and recall rates in the second comparison might have been dominated by the de novo gene boundaries and exon loci that are different from the annotation. Therefore, we performed a third comparison between SLIDE and Cufflinks with only the genes whose de novo assembled exons agree with annotated exons in their loci. We found that the precision and recall rates of SLIDE are higher than those of Cufflinks. Therefore, we concluded that the isoform discovery performance of SLIDE is better than, or at least comparable to, that of Cufflinks.

The comparison results in the main paper are based on dataset 1 (Table 1 in the main paper). We did the same set of comparisons on datasets 2–4 (Table 1 in the main paper), and the results are summarized in Figs. S4 and S5 (results on dataset 1 are in Fig 2 *B* and *C* of the main paper). From Figs. S4 and S5, we observe that the comparison results on datasets 2–4 are consistent with the results on dataset 1.

3.2. Comparison between SLIDE and IsoLasso/NSMAP. Here, we compare SLIDE with two other isoform discovery methods with lasso-type sparse estimation: IsoLasso (5) and NSMAP (6).

SLIDE is different from IsoLasso (5) in three aspects. (*i*) IsoLasso enumerates isoforms based on a connectivity graph used by Scripture (10). This deterministic approach finds the longest paths indicated by connected paired-end reads and would not consider isoforms with alternative starts/ends (i.e., one isoform is a fragment of the other) as isoform candidates. (*ii*) IsoLasso uses a binary design matrix to relate reads to isoforms. It does not fully capture the quantitative relationship between read counts and isoform abundance. In contrast, our design matix uses conditional probabilities to relate read counts to isoform abundance, and is flexible in terms of incorporating different types of biological information into the modeling (e.g., using GC content to adjust nonuniform read coverage). (*iii*) IsoLasso performs isoform discovery and abundance estimation simultaneously with Lasso, a sparse estimation method. However, the penalization term in Lasso would introduce biases to the abundance estimates. To fix this issue, SLIDE uses a two-step approach that first discovers isoforms by sparse estimation and subsequently estimates the abundance of the discovered isoforms by nonnegative least squares that gives less biased estimates than Lasso does. (*iv*) Unlike IsoLasso, SLIDE favors isoforms with more exons in its sparse estimation. This is because we observe that RNA-Seq data noise often leads the linear model to fit with multiple isforms each with a small numbers of exons, contradicting with annotations. To counteract such data noise, we give less penalty to isoforms with more exons in the sparse estimation. In addition, IsoLasso builds isoform candidates from de novo exons directly assembled by mapped reads, without taking annotated gene and exon information into account.

We conducted three numerical comparisons between SLIDE and IsoLasso on isoform discovery based on the same data used in the comparison between SLIDE and Cufflinks. In the first comparison, we evaluated both methods in their default settings, where SLIDE builds isoforms from exons in UCSC annotations and IsoLasso finds isoforms from its de novo assembled exons. The discovered isoforms by either method are evaluated by UCSC annotations, where a discovered isoform is called to match an annotated isoform if they have the same number of exons and all of their exons overlap. Thus, this evaluation scheme is not sensitive to exon boundaries as long as a discovered isoform has exons in the same loci as exons of an annotated isoform. Precision and recall rates are calculated as described in the main paper. The comparison results in Fig. S6*A* show that SLIDE has better precision and recall rates than IsoLasso does. These results are similar to the first comparison results between SLIDE and Cufflinks in the main paper. The main reason is that both IsoLasso and Cufflinks find isoforms for de novo assembled genes, whose boundaries are sensitive to RNA-Seq data noise, especially to biases of junction read counts. These results suggest the importance of scrutinizing de novo assembled genes and exons with available annotations before performing isoform discovery; however, because SLIDE and IsoLasso do not start from the same set of genes and exons, this comparison is not a fair evaluation of their isoform assembly performance. Thus, we performed a second comparison based on isoforms discovered by either method from de novo genes and exons assembled by IsoLasso. Fig. S6*B* shows that SLIDE still has better precision rates than IsoLasso has for most genes. To further exclude the effects of disagreement between annotated and de novo assembled exons, we carried out a third comparison of the two methods using only the de novo assembled exons that agree with the annotation. We found that SLIDE has an average precision rate 0.85 and recall rate 0.91, whereas IsoLasso has an average precision rate 0.79 and recall rate 0.91. This again shows that SLIDE has higher precision than IsoLasso has in isoform assembly from the same set of de novo exons.

NSMAP is a Bayesian model-based method that estimates the abundance of isoform candidates as MAP (maximum a posteriori) estimates (6). It is an extension of the maximum-likelihood abundance estimation method “statistical inferences for isoform expression in RNA-Seq” (SIIER) (11), in the sense of expanding parameters of interest from the abundance of annotated isoforms to that of all isoform candidates. NSMAP uses a Laplace prior to introduce sparseness and then discovers isoforms based on MAP estimates of the abundance of isoform candidates. NSMAP is similar to IsoLasso in four aspects. (*i*) Both methods use deterministic approaches to construct isoform candidates. NSMAP uses the minimal set of isoforms that can explain all junction reads, and it would miss isoforms with alternative starts/ends (i.e., one isoform is a fragment of the other) in its isoform candidate set. (*ii*) NSMAP is equivalent to IsoLasso in the optimization step. In the original Lasso paper, it was suggested that Lasso estimates can be interpreted as posterior mode estimates when the regression parameters have independent and identical Laplace priors (3). Unlike SLIDE, both NSMAP and IsoLasso do not favor isoforms with more exons in their sparse estimation, but they only keep the longest isoforms in their candidate sets. (*iii*) Both methods perform isoform discovery and abundance estimation simultaneously with sparse estimation. (*iv*) Both methods build isoforms from de novo assembled genes and exons. NSMAP constructs genes and exons de novo from read alignment output of Tophat. Therefore, the differences between SLIDE and NSMAP in methodology would be similar to those between SLIDE and IsoLasso. We tried to conduct numerical comparison between SLIDE and NSMAP. However, a code bug in the NSMAP package (Version 0.1.0) prohibited us from using it, and our attempts at contacting the authors were not successful.

4. More About mRNA Isoform Abundance Estimation on modENCODE Data. To evaluate the isoform abundance estimation accuracy of SLIDE without knowing the ground truth of isoform quantities in datasets 1–4, we compare SLIDE to two widely used methods: statistical inferences for isoform expression in RNA-Seq (SIIER) (11) and Cufflinks (1). All three methods are used to estimate the isoform proportions of 317 chr3R genes with multiple isoforms in the UCSC annotation, and the total number of isoforms is 798. On dataset 1, the SLIDE and SIIER estimates have a correlation $R = 0.75$, and there are 25 genes with significantly inconsistent estimates between the two methods; i.e., $\hat{p}_{\mathrm{SLIDE}} < 0.1$ and $\hat{p}_{\mathrm{SIIER}} > 0.5$ or $\hat{p}_{\mathrm{SLIDE}} > 0.5$ and $\hat{p}_{\mathrm{SIIER}} < 0.1$. By detailed manual inspection, we find that among the 25 genes there are 20 genes whose SLIDE estimates agree better with the paired-end bin counts. For example, gene *CG9801* has five subexons with RPKMs 8.25, 5.57, 0, 3.92, and 3.16, respectively, and observed junctions between subexons 1–2, 2–4, and 4–5 in dataset 1. There are three isoforms (1,2), (1,2,5), and (1,2,4,5) of *CG9801* in the annotation. SLIDE estimates their proportions as 0.76, 0, and 0.24, respectively, whereas SIIER’s estimates are 0, 0.55, and 0.45, respectively. Because there is no observed junction between subexons 2 and 5 and the expression levels of subexons 1 and 2 are higher than those of subexons 4 and 5, the SLIDE estimates seem more consistent with the data. The rest of the 25 genes include one gene whose SIIER estimates agree better with the paired-end bin counts, and four genes with ambiguous bin counts that cannot differentiate the two sets of estimates. An example of the ambiguous cases is gene *D1* with five subexons. In dataset 1, the RPKMs of the five subexons are 327.79, 326.01, 16.6, 6.23, and 0, respectively, and there are observed junction reads between subexons 1–2, 2–3, and 3–4. SLIDE estimates the proportions of annotated isoforms (1,2,3,4) and (1,2,3) as 0.02 and 0.98, respectively, whereas SIIER returns estimates 1 and 0, respectively. Based on the annotation, we would expect subexons 1, 2, and 3 to have similar expression levels; however, the observed expression in subexon 3 is significantly lower than that of subexons 1 and 2. So the data seriously contradicts with the annotation. Hence, both SLIDE and SIIER cannot reasonably fit the data based on the annotation. After removing those 25 genes, we have a correlation $R = 0.88$ between the SLIDE and SIIER estimates.

In the comparison between SLIDE and Cufflinks, the correlation between their estimates on the proportions of the 798 isoforms is $R = 0.67$ on dataset 1. Similarly, we find 35 genes with significantly inconsistent estimates between SLIDE and Cufflinks, $\hat{p}_{\mathrm{SLIDE}} < 0.1$ and $\hat{p}_{\mathrm{Cufflinks}} > 0.5$ or $\hat{p}_{\mathrm{SLIDE}} > 0.5$ and $\hat{p}_{\mathrm{Cufflinks}} < 0.1$. Again by detailed manual inspection, we observe that 30 of them have SLIDE estimates that agree better with the paired-end bin counts, 3 have Cufflinks estimates that agree with the bin counts, and 2 have ambiguous bin counts such that both estimates are reasonable. After removing those 35 genes, we have a correlation $R = 0.85$ between the SLIDE and Cufflinks estimates.

5. More About the Exploration of Read/Fragment Length Effect. In the exploration of whether different read lengths would affect the isoform discovery results of SLIDE, we applied SLIDE to datasets 2 and 3, which are from the same Kc167 sample, with similar sequencing depth, but of read lengths 37 and 76 bp, respectively. Surprisingly, the precision and recall rates on the 37-bp data are higher than those on the 76-bp data. In the search for a possible explanation, we observed that the cDNA fragments in single-exon genes have different fragment length distributions in the two datasets: $N(166,26^2)$ and $N(127,13^2)$ for the 37-bp and 76-bp data, respectively.

To explore whether the read length or the fragment length has larger effects on the isoform discovery, we did a simulation study with two different read lengths (37 and 76 bp) and three different fragment length ranges (50–100 bp, 100–150 bp, and 150–200 bp). In each of the 50 simulation runs, 500 paired-end RNA-Seq reads are generated in each setting for each read length and each fragment length range. We applied SLIDE to the simulated data and summarized the precision and recall rates of each setting in Fig. S7,. The figure illustrates that the increase in fragment lengths from 50–100 bp to 100–150 bp significantly improves the precision and recall rates of isoform discovery. Changes in fragment lengths from 100–150 bp to 150–200 bp also improve the precision and recall rates by increasing their means to some extent and decreasing the width of their confidence intervals. Compared to the fragment length changes, read length changes from 37 bp to 76 bp have smaller effects on the isoform discovery results.

6. Read Coverage vs. GC Content. It has been reported by several groups that read coverage has a strong correlation with GC content in high-throughput DNA sequencing data (2, 12). As high-throughput sequencing technologies (e.g., DNA sequencing, RNA-Seq, ChIP-Seq, etc.) have similar characteristics in the sequencing step, many researchers believe that a strong correlation between read coverage and GC content also exists in RNA-Seq data (13, 14). However, unlike DNA sequencing data, RNA-Seq read coverage varies in different transcribed regions and is mainly determined by expression levels and alternative splicing patterns of the regions (15). It would be difficult to compare read coverage across subexons, which may occur in different transcripts and thus have different expression levels. To check the validity of using GC content correction in our SLIDE model, we study the relationship between RNA-Seq read coverage and GC content within subexons, using RNA-Seq reads on chr3R in dataset 1 (see Table 1 of the main paper). We use three different window sizes: 10 bp, 30 bp, and 50 bp. For every subexon, we calculate the correlation coefficient of its windowed average read coverage vs. GC content. Then, we calculate the percentage of subexons giving positive correlations among all the subexons with more than n windows ($n = 3,10,\ldots,100$), and find that the percentage increases as n increases. This trend is observed with all the three window sizes. The percentages for 10-bp windows are summarized in Table S2. A histogram of the correlations in subexons with more than 100 windows is in Fig. S8. Because we expect that correlations calculated in subexons with more windows can better represent the relationship between read coverage and GC content, we conclude that there is a positive correlation between read coverage and GC content.

7. Some Other Details in the Analysis.

- In the simulation study of the main paper, we simulated reads from the 1,972 genes of 3–10 subexons (defined in the main paper) on chr3R from *D. melanogaster* annotation (September 2010) of UCSC Genome Browser (16). For each gene, reads are generated from the annotated isoforms, whose proportions p_k are randomly sampled from $\{0,0.1,\cdots,0.9,1\}$ subject to the constraint that $\sum_k p_k = 1$. For every gene, we simulate 500 reads in each run, with 50 runs in total.
- In the sparse estimation, we selected an optimal λ for each group of genes with n subexons ($n = 3,\cdots,10$) by a stability criterion (7). However, there are a small number of genes where zero isoforms were identified under the selected λ. For those genes, we reselected a gene-specific λ. In more details, we replace the previous λ by $\lambda^* = \max(\lambda - 0.1,\lambda/2)$ until nontrivial results were obtained.
- For isoform discovery, SLIDE uses sparse linear model estimation to find isoforms. We note that the linear model for paired-end data (Eq. **3** in the main paper) is identifiable; i.e. $\mathbf{F}^T\mathbf{F}$ is invertible (8), for a few genes with 3–10 subexons of *D. melanogaster* (Table S1). In those cases, we additionally attempted to use nonnegative least squares (NNLS), whose estimation results should be less biased than those of L_1 penalized estimation. However, compared to the penalized estimation results in the main paper, we found that the NNLS results include a lot of short isoforms as truncated fragments of isoforms in the UCSC annotation. In the example of gene *jumu*, whose three subexons have RPKMs 20.86, 42.62, and 25.97, respectively, there are observed junctions between subexons 1–2 and 2–3. NNLS discovered isoforms (1,2), (2,3), and (1,2,3) for *jumu*, whereas SLIDE only found the longest isoform (1,2,3), which agrees with the annotation. The possible reason of NNLS finding short isoforms is that RNA-Seq data have unexpected read coverage variation among exons in the same transcript (12–14).

1. Trapnell C, et al. (2010) Transcript assembly and quantification by RNA-Seq reveals unannotated transcripts and isoform switching during cell differentiation. *Nat Biotechnol* 28:511–515.
2. Hiller D (2010) Alternative splicing analysis using RNA-seq data. PhD dissertation (Department of Statistics, Stanford University, Palo Alto, CA).
3. Tibshirani R (1996) Regression shrinkage and selection via the lasso. *J R Stat Soc Series B Stat Methodol* 58:267–288.
4. Dahinden C, Parmigiani G, Emerick MC, Bhlmann P (2007) Penalized likelihood for sparse contingency tables with an application to full-length cDNA libraries. *BMC Bioinformatics* 8:1–11.
5. Li W, Feng J, Jiang T (2011) IsoLasso: A LASSO regression approach to RNA-Seq based transcriptome assembly. *15th Annual International Conference on Research in Computational Molecular Biology (RECOMB 2011), Lecture Notes on Computer Science* (Springer, Berlin/Heidelber), 6577:168–188.
6. Xia Z, Wen J, Chang C, Zhou X (2011) NSMAP: A method for spliced isoforms identification and quantification from RNA-Seq. *BMC Bioinformatics* 12: 162.
7. Meinshausen N, Bühlmann P (2010) Stability selection. *J R Stat Soc Series B Stat Methodol* 72:417–473.
8. Hiller D, Jiang H, Xu W, Wong WH (2009) Identiability of isoform deconvolution from junction arrays and RNA-Seq. *Bioinformatics* 25:3056–3059.
9. Zheng S, Chen L (2009) A hierarchical Bayesian model for comparing transcriptomes at the individual transcript isoform level. *Nucleic Acids Res* 37:e75.
10. Guttman M et al. (2010) Ab initio reconstruction of cell typespecific transcriptomes in mouse reveals the conserved multi-exonic structure of lincRNAs. *Nat Biotechnol* 28:503–510.
11. Jiang H, Wong WH (2009) Statistical inferences for isoform expression in RNA-Seq. *Bioinformatics* 25:1026–1032.
12. Dohm JC, Lottaz C, Borodina T, Himmelbauer H, (2010) Substantial biases in ultra-short read data sets from high-throughput DNA sequencing. *Nucleic Acids Res* 36: e105.
13. Hansen KD, Brenner SE, Dudoit S (2010) Biases in Illumina transcriptome sequencing caused by random hexamer priming. *Nucleic Acids Res* 38: e131.
14. Li J, Jiang H, Wong WH (2010) Modeling non-uniformity in short-read rates in RNA-Seq data. *Genome Biol* 11: R50.
15. Srivastava S, Chen L (2010) A two-parameter generalized Poisson model to improve the analysis of RNA-seq data. *Nucleic Acids Res* 38: e170.
16. Fujita PA (2011) The UCSC Genome Browser database: Update 2011. *Nucleic Acids Res* 39(Suppl 1):D876–D882.

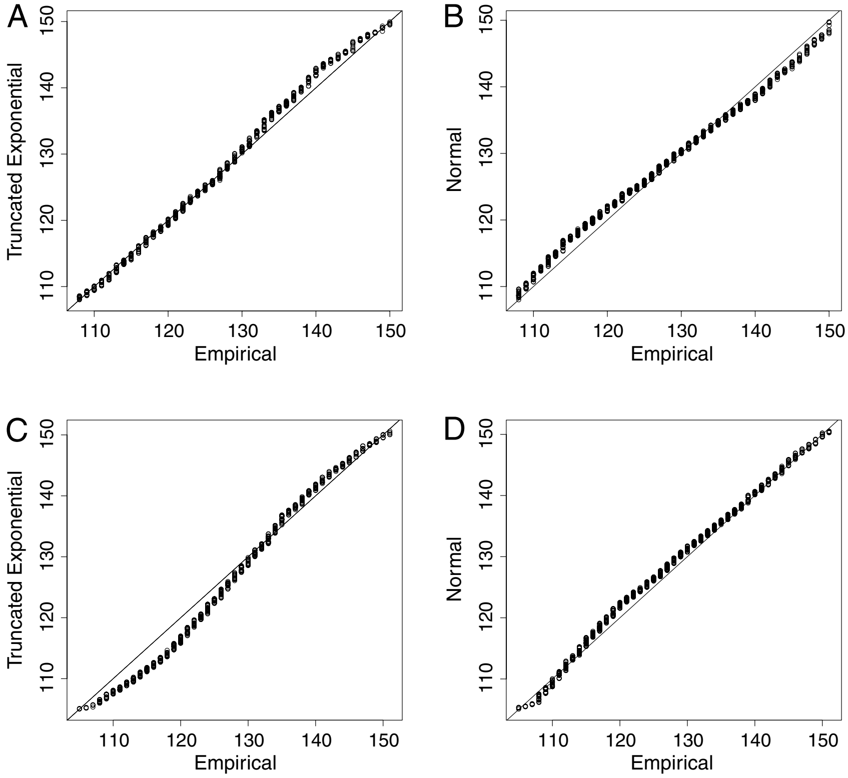

Fig. S1. Q-Q plots of modeled vs. empirical fragment length distribution on dataset 1. Note that only the fragment lengths between the 5% and 95% percentiles of the empirical distribution are used to construct the Q-Q plots, because extremely long or short fragments may be results of mapping errors. (*A*) Q-Q plot of truncated Exponential distribution vs. empirical length distribution of cDNA fragments within single-exon genes. (*B*) Q-Q plot of Normal distribution vs. empirical length distribution of cDNA fragments within single-exon genes. (*C*) Q-Q plot of truncated Exponential distribution vs. empirical length distribution of cDNA fragments within single-isoform genes. (*D*) Q-Q plot of Normal distribution vs. empirical length distribution of cDNA fragments within single-isoform genes.

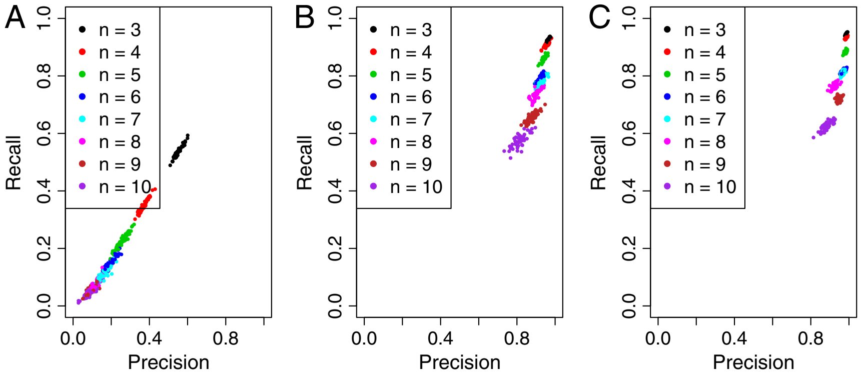

Fig. S2. Precision and recall rates of SLIDE on simulated data with different read coverages. (*A*) Read coverage is 10 reads per kilobase. (*B*) Read coverage is 50 reads per kilobase. (*C*) Read coverage is 100 reads per kilobase.

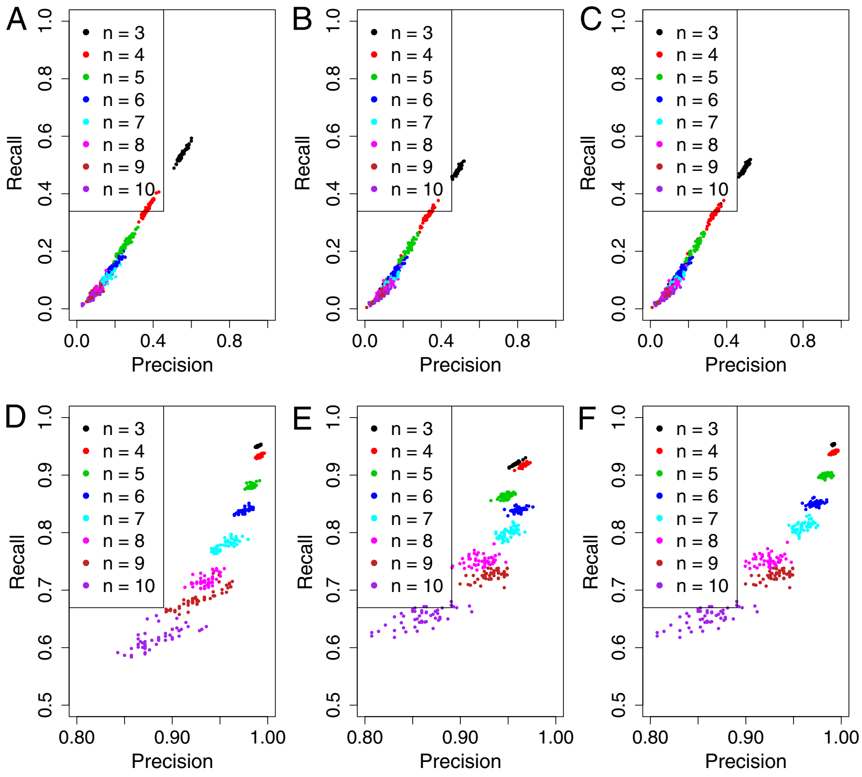

Fig. S3. Precision and recall rates of SLIDE using different likelihoods in simulation with two different read coverages. (*A*) Normal likelihood, (*B*) Poisson likelihood, and (*C*) multinomial likelihood (logistic regression) with read coverage 10 reads/kb. (*D*) Normal likelihood, (*E*) Poisson likelihood, and (*F*) multinomial likelihood (logistic regression) with read coverage 100 reads/kb.

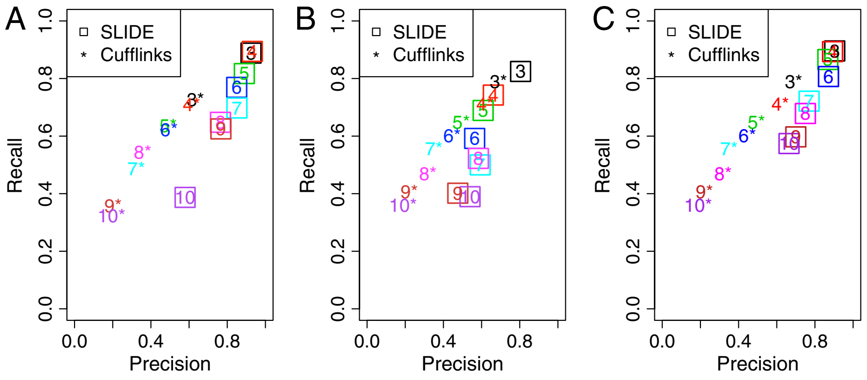

Fig. S4. Comparison of isoform discovery results by SLIDE (using genes and exons from the UCSC annotation) and Cufflinks. (*A*) Precision and recall rates of SLIDE and Cufflinks on dataset 2. The numbers in the figure are the group indices of genes (i.e., numbers of subexons). The squares and stars represent SLIDE and Cufflinks results, respectively. (*B*) Precision and recall rates of SLIDE and Cufflinks on dataset 3. The numbers, squares, and stars have the same meaning as in *A*. (*C*) Precision and recall rates of SLIDE and Cufflinks on dataset 4. The numbers, squares, and stars have the same meaning as in *A*.

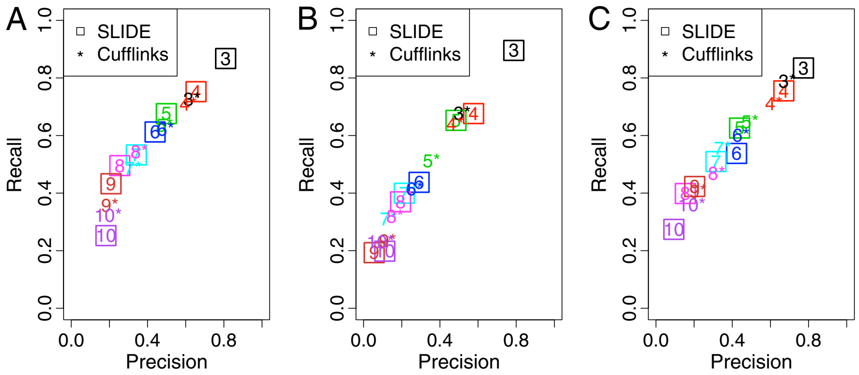

Fig. S5. Comparison of isoform discovery results by SLIDE (using de novo genes and exons assembled by Cufflinks) and Cufflinks. (*A*) Precision and recall rates of SLIDE and Cufflinks on dataset 2. The numbers in the figure are the group indices of genes (i.e., numbers of subexons). The squares and stars represent SLIDE and Cufflinks results, respectively. (*B*) Precision and recall rates of SLIDE and Cufflinks on dataset 3. The numbers, squares, and stars have the same meaning as in *A*. (*C*) Precision and recall rates of SLIDE and Cufflinks on dataset 4. The numbers, squares, and stars have the same meaning as in *A*.

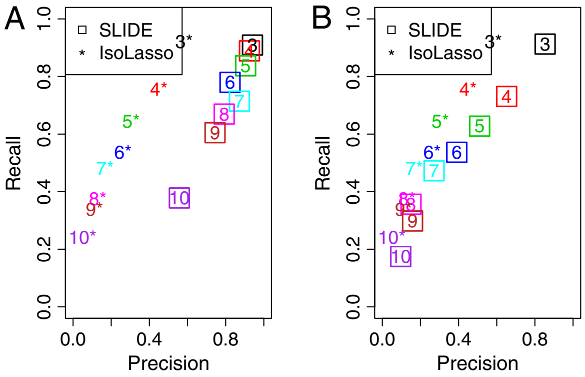

Fig. S6. Comparison of isoform discovery results by SLIDE and IsoLasso. (*A*) Precision and recall rates of SLIDE (using annotated genes/exons) and IsoLasso on dataset 1. The numbers in the figure are the group indices of genes (i.e., numbers of subexons). The squares and stars represent SLIDE and Cufflinks results, respectively. (*B*) Precision and recall rates of SLIDE (using IsoLasso assembled genes/exons) and IsoLasso on dataset 1. The numbers, squares, and stars have the same meaning as in *A*.

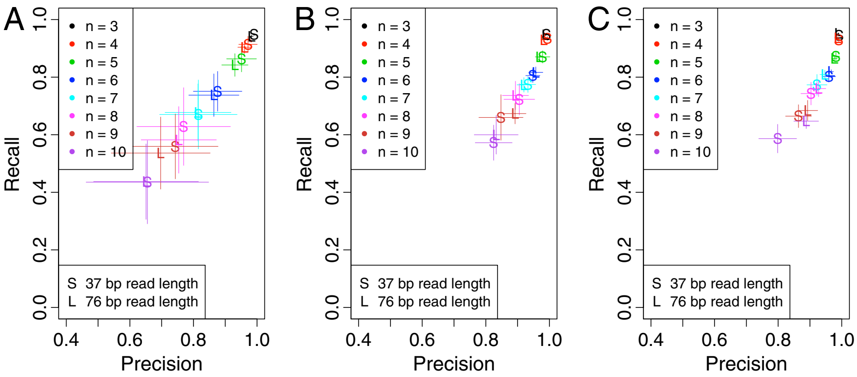

Fig. S7. Simulation study of read/fragment length effects on isoform discovery. (*A*) Precision and recall rates of SLIDE on simulated paired-end RNA-Seq data with fragment lengths in the range of 50–100 bp and two different read lengths (37 bp vs. 76 bp). 95% confidence intervals of precision and recall rates are shown as error bars parallel to the *x* and *y* axes, respectively. (*B*) Precision and recall rates of SLIDE on simulated paired-end RNA-Seq data with fragment lengths in the range of 100–150 bp and two different read lengths (37 bp vs. 76 bp). The confidence intervals are shown in the same way as in *A*. (*C*) Precision and recall rates of SLIDE on simulated paired-end RNA-Seq data with fragment lengths in the range of 150–200 bp and two different read lengths (37 bp vs. 76 bp). The confidence intervals are shown in the same way as in *A*.

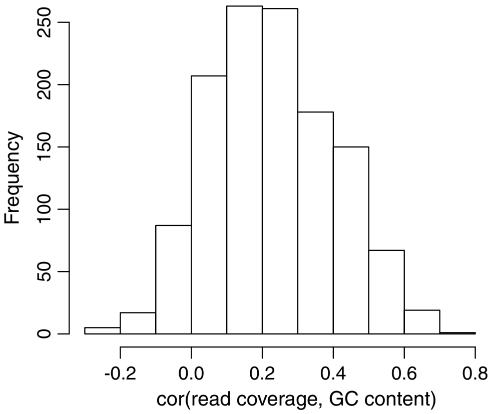

Fig. S8. A histogram of correlations between windowed read coverage and GC content in subexons with more than 100 windows of 10-bp size.

Table S1. Number of genes with unidentifiability issues before and after preselection procedures

No. of subexons	Total no. of genes	No. of genes with unidentifiability issue before the preselection procedures	No. of genes with unidentifiability issue after the preselection procedures
3	295	204 (69.2%)	1 (0.3%)
4	237	228 (96.2%)	198 (83.5%)
5	165	165 (100%)	155 (93.9%)
6	142	142 (100%)	137 (96.5%)
7	82	82 (100%)	80 (97.6%)
8	72	72 (100%)	70 (97.2%)
9	56	56 (100%)	55 (98.2%)
10	35	35 (100%)	35 (100%)

Table S2. Percentages of subexons (>*n* 10-bp windows) with positive correlation (R) between read coverage and GC content

n	3	10	20	40	60	80	100
Percentage	77.3%	78.6%	83.0%	87.9%	90.1%	91.0%	91.3%
Mean(R)	0.171	0.174	0.193	0.219	0.227	0.232	0.229